

Peer review status:

This is a non-peer-reviewed preprint submitted to EarthArXiv.

Spaceborne mineral mapping reduces dust's shortwave radiative impact uncertainty

Longlei Li^{1*}, Natalie M. Mahowald^{1*}, Ron L. Miller², Carlos Pérez García-Pando^{3,4},
María Gonçalves Ageitos^{3,5}, Paul Ginoux⁶, Vincenzo Obiso³, Qianqian Song⁷, Philip G.
Brodrick⁸, David R. Thompson⁸, Roger N. Clark⁹, Gregory S. Okin¹⁰, Bethany L.
Ehlmann¹¹, Bo Zhou¹⁰, Olga Kalashnikova⁸, and Robert O. Green⁸

1. Department of Earth and Atmospheric Sciences, Cornell University, Ithaca, NY, United States
2. NASA Goddard Institute for Space Studies, New York, NY, United States
3. Barcelona Supercomputing Center, Barcelona, Spain
4. ICREA, Catalan Institution for Research and Advances Studies, Barcelona, Spain
5. Department of Project and Construction Engineering, Universitat Politècnica de Catalunya – Barcelona Tech, Terrassa, Spain
6. NOAA/OAR Geophysical Fluid Dynamics Laboratory, Princeton, NJ, United States
7. GESTAR-II, University of Maryland, Baltimore County, MD, United States
8. Jet Propulsion Laboratory, California Institute of Technology, Pasadena, CA, United States
9. Planetary Science Institute, Tucson, AZ, United States
10. University of California Los Angeles, Los Angeles, CA, United States
11. California Institute of Technology, Pasadena, CA, United States

*Longlei Li and Natalie M. Mahowald

Email: ll859@cornell.edu (l.longlei@gmail.com) and mahowald@cornell.edu

This paper has been submitted to Nature Geoscience.

Abstract

Mineral dust impacts climate through complex interactions with radiation, which remain poorly quantified due to uncertainties in the amount of light-absorbing iron oxides within dust particles. NASA's EMIT imaging spectrometer, now delivering high-resolution soil mineralogy from the International Space Station, provides the first observational basis to address this gap at a global scale. Using the EMIT data within Earth system model ensembles, we show that surface composition retrievals, especially of iron oxides, reduce uncertainty in the dust shortwave direct radiative effect by over 50% for both present-day and late-21st-century climates. The greatest improvements occur over the Sahara, where the regional dust concentration is high and dust radiative impacts are simulated with improved fidelity. While uncertainties remain, EMIT shifts the primary uncertainty source from mineralogical composition to our imprecise knowledge of the processes controlling the mass concentration of dust particles, especially those related to emission. These findings represent a pivotal step toward mineral-resolved dust aerosol modeling, offering improved insight into how dust alters Earth's energy balance today and in a warming future.

Main

Mineral dust, Earth's most abundant atmospheric aerosol by mass¹, causes a complex, yet poorly quantified, influence over climate². From perturbing the planet's radiation budget³ to affecting cloud microphysics⁴ and fertilizing marine ecosystems^{5,6}, dust interacts with nearly every Earth system component. Nowhere is this influence more pronounced than in major source regions such as the Sahara, Middle East, and East Asia, where vast quantities of soil particles are lofted into the atmosphere¹. However, a critical obstacle remains in quantifying the dust direct radiative effect (DRE), which strongly depends on the soil mineralogical composition⁷⁻¹⁰ and, by extension, its optical properties.

Unlike purely scattering aerosols such as sulfates¹¹, dust particles both absorb and scatter shortwave (SW) and longwave (LW) radiation^{3,12}. This complicated interaction renders their net radiative impact especially complex, as the balance between warming and cooling is dictated by multiple factors¹³, including the abundance of iron oxides such as hematite and goethite⁷⁻¹⁰. These minerals strongly absorb SW radiation, and their atmospheric abundance varies dramatically across space and time^{14,15}. Yet until recently, Earth system models (ESMs) have been ill-equipped to capture this mineralogical variability: Existing soil mineral atlases^{14,15} were derived from sparse soil samples, often unrepresentative of soils in dust source regions. This limitation leaves the SW DRE with a large uncertainty range of -0.23 to +0.28 W m⁻², much of which is traced to the treatment of mineralogy⁷.

EMIT¹⁶ has fundamentally changed this landscape. Using a high-resolution imaging spectrometer operating from its vantage point on the International Space Station (ISS), EMIT has mapped the mineralogical composition of Earth's arid and semiarid

surfaces comprehensively at high spatial resolution^{17–20}, providing the first global-scale observational dataset capable of resolving spatial patterns of dust-relevant minerals, including iron oxides^{21,22} (Methods). These improvements are important for understanding the dust DRE, especially in the context of future climate. As warming and land use changes alter wind patterns, vegetation cover, and arid landscapes, the sources and thus the mineralogical composition of dust aerosols are expected to shift^{23,24}, which may cause changes that pre-EMIT soil atlases (C1999¹⁴ and J2014¹⁵) cannot capture with high accuracy. EMIT’s constraints arrive at a pivotal moment, providing a foundation for developing the next generation of ESMs that explicitly resolve this issue. For example, EMIT can provide the mineralogical composition of projected future dust sources with fidelity. With this information, the scientific community now can redefine how mineral dust is represented in ESMs^{7,25–28}.

Here, we incorporate EMIT-derived mineralogical atlases²⁹ (see “Data availability”) into an ensemble of four ESMs (Methods) to provide the first observationally constrained estimate of the SW DRE under all-sky conditions at the top of the atmosphere (a level definition consistently applied here and elsewhere) for both the present day and the late 21st century. We compare these results with estimates derived from the pre-EMIT soil atlases^{14,15} using the same methodology. A natural question is whether the leap in mineralogical detail provided by EMIT translates to better agreement between models and observations of dust radiative properties. To answer this question, we compare simulations using the EMIT soil atlas against satellite-derived DRE efficiency (DREE; defined as the DRE divided by the dust extinction at visible wavelengths; Methods).

By grounding simulations in observationally constrained soil mineralogical composition, we demonstrate that EMIT data reduce uncertainty in the dust SW DRE by over 50% for both present-day and late-21st-century climates, which represents a significant advance. This reduction is most pronounced over high-albedo desert regions, where dust SW absorption plays an important role in its radiative impact³⁰. The EMIT data thus both sharpen our understanding of dust’s role in present-day climate processes and strengthen our capacity to predict future climate trajectories.

This work enables a key turning point in Earth system science in the context of dust: the transition from bulk representations of mineralogically homogeneous dust, which fail to capture the spatial variability of dust aerosols’ optical properties³¹ and their climatic impacts, to a nuanced, mineral-resolved modeling of its interaction with radiation^{7,27,32}. As ESMs evolve to include ever more biogeochemical realism, including the impact of specific dust minerals upon ocean primary productivity, our findings demonstrate how targeted Earth observations can close longstanding

knowledge gaps, and, in doing so, reshape our understanding of one of the most enigmatic agents of atmospheric change.

EMIT unlocks the mineral fingerprint of global dust

Leveraging measurements from a cutting-edge imaging spectrometer operating from its vantage point on the ISS and the Tetracorder algorithm²⁰, EMIT mosaicked cloud-free observations from August 2022 to October 2024 to generate estimates of key minerals relevant to the dust SW DRE, including hematite and goethite, at the instrument's native 60-meter resolution (Methods). These data were processed with rigorous quality control on input reflectance, particle size attribution, and uncertainty quantification (95% confidence interval; Methods), then aggregated to 0.5° spatial resolution for use in ESMs. Validated against in situ measurements^{20,33} and covering nearly all major dust-emitting regions, the EMIT atlas provides a foundation for physically based simulations of dust aerosols and their climate impacts.

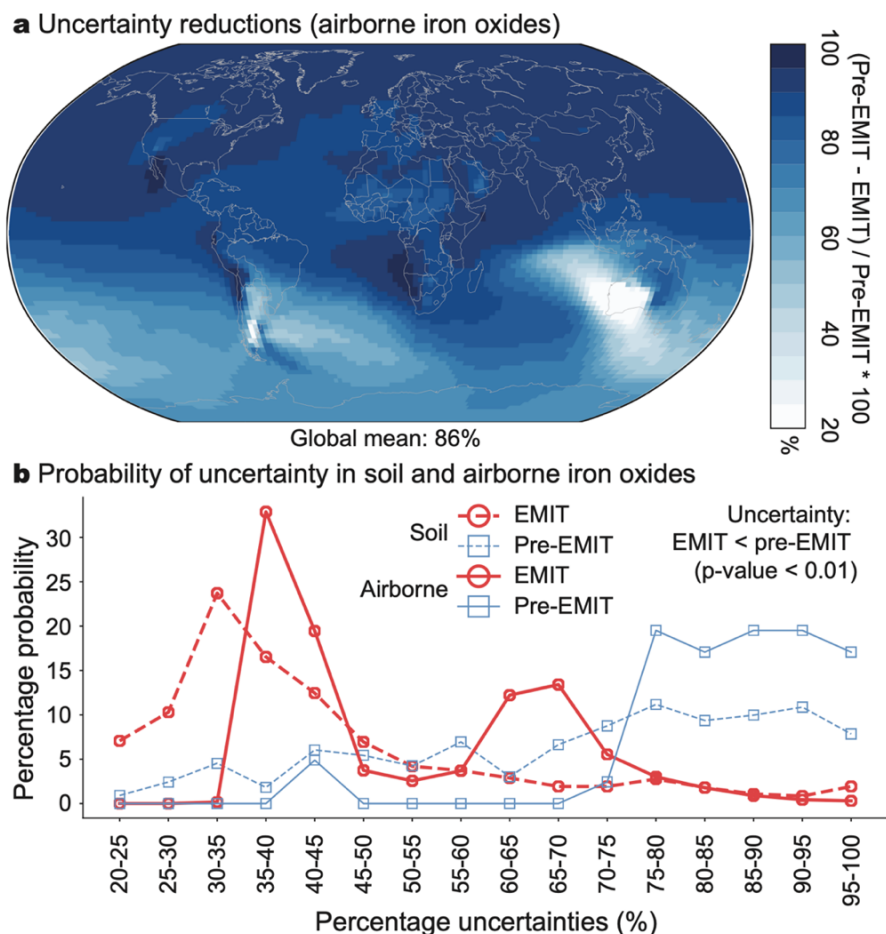


Figure 1. Improved representation of iron oxides with EMIT. a, Ensemble-mean 95% confidence intervals for airborne iron oxides in the present-day climate simulated by CESM2 and ModelE, showing the reduction of uncertainty resulting

from EMIT compared with pre-EMIT soil mineral atlases from Claquin et al.¹⁴ (C1999) and Journet et al.¹⁵ (J2014). **b**, Probability distributions of uncertainties in soil and simulated airborne iron oxides. The EMIT uncertainty is significantly lower than the pre-EMIT uncertainty (one-sided Mann-Whitney U test, p-value < 0.01).

Our analysis suggests that EMIT's first map of soil iron oxides significantly improves our ability to track these minerals in both soils and the atmosphere, which is critical for estimating the dust SW DRE. Where earlier estimates of the soil iron oxides had uncertainties exceeding 75%, EMIT cuts these to under 45% across most regions (Fig. 1b; Supplementary Fig. 1; Methods). This leap in precision ripples through climate simulations: when fed into Community ESM version 2 (CESM2) and ModelE (Methods), EMIT's soil data reduce uncertainty in airborne iron oxide content by over 80% in most dust-prone areas (Fig. 1a).

EMIT advances knowledge of dust optical properties

The precision and global comprehensiveness of EMIT's hyperspectral retrievals¹⁷ are reflected in a significant narrowing of uncertainty. The comparison of the modeled clear-sky SW DREE with satellite-based retrievals at the top of the atmosphere (Fig. 2) also suggests a clear signal: EMIT-derived soil iron oxides allow the models to simulate the dust clear-sky SW DREE with dramatically tighter uncertainty ranges than previously possible (Fig. 2). This improvement is seen over the Sahara Desert, the planet's largest source of dust aerosols¹, which dominates global dust absorption of SW radiation³⁴. In CESM2, EMIT reduces SW DREE error over this desert by 80%, yielding values that fall within observationally constrained ranges. Across the four ESMs with diverse aerosol size treatments and radiative transfer schemes, EMIT fosters convergence in the SW DREE estimates within $\pm 2.0 \text{ W m}^{-2} \tau^{-1}$ (τ , a unitless measure of optical depth at visible wavelengths) over the Sahara Desert, compared to the $\sim 20 \text{ W m}^{-2} \tau^{-1}$ difference among these ESMs using the pre-EMIT data. This accomplishment underscores the dominant role of iron oxides in determining the SW DREE and highlights the more confident estimates of iron oxides made possible by EMIT.

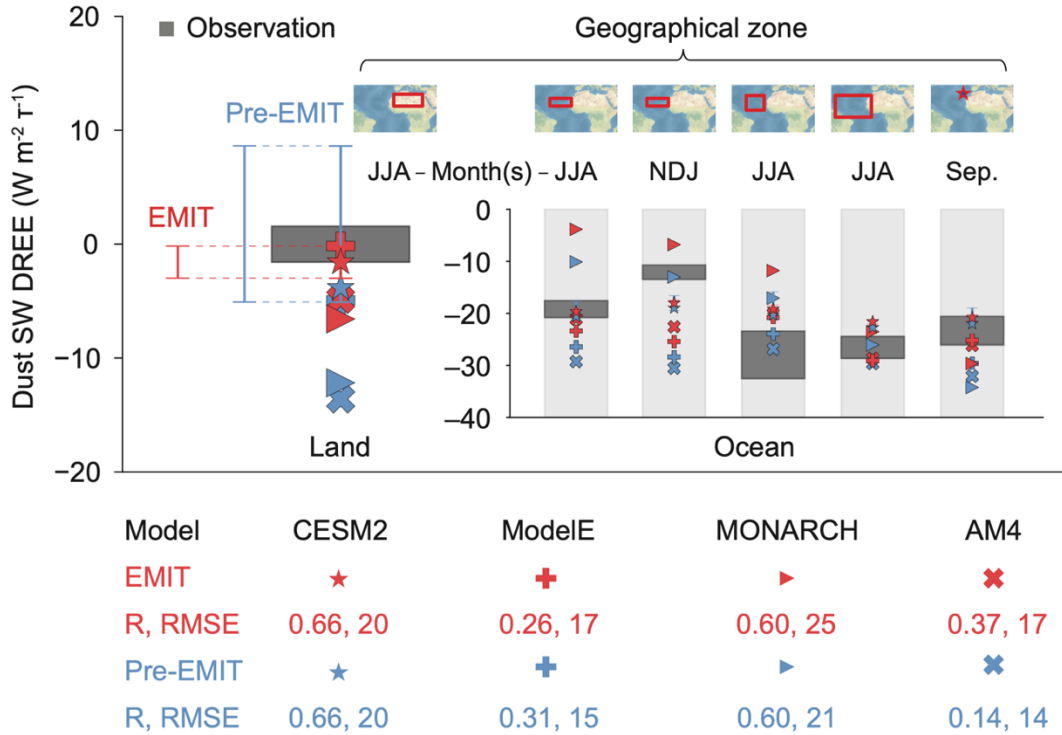


Figure 2. EMIT improves the modeling of the dust shortwave (SW) direct radiative effect efficiency (DREE). Simulated daily mean dust SW DREE at the top of the atmosphere using EMIT and pre-EMIT soil atlases (clear-sky for CESM2; all-sky for the other ESMs: See Methods), compared with satellite-based retrievals (grey bars). Daytime mean estimates from observations have been adjusted to represent daily means (Methods). Error bars correspond to the CESM2 simulations; they are asymmetric error bars for the simulations using pre-EMIT atlases; this results from more absorbing dust in the simulation with the J2014 soil atlas¹⁵, due to its higher iron oxide content compared to the C1999 atlas¹⁴. Spatial correlation (R) and root mean square error (RMSE; unit: $\text{W m}^{-2} \tau^{-1}$) are calculated across the six regions with equal weighting.

While we focus on CESM2 for clarity, similar improvements are expected in the other models (e.g., Fig. 2). This tightening of uncertainty ranges is driven by EMIT's improved characterization of iron oxide content (Fig. 1), specifically hematite and goethite, which are powerful absorbers in the SW spectrum. Sensitivity analyses confirm that uncertainty in the iron oxide mass fraction, as represented by pre-EMIT soil atlases, is the primary driver of modeled SW DRE range across experiments (Fig. 3, Supplementary Figs. 2-3).

On a global scale, EMIT does not drastically alter mean estimates of present-day SW DRE, which remain within previously reported ranges^{7,35} (however, below, we note a reduction in uncertainty due to EMIT). EMIT also does not lead to a significant revision in the projected change in the dust SW DRE from the present day to the late

21st century (Fig. 3a). Nonetheless, EMIT introduces notable changes in regional and monthly global values (Supplementary Figs. 4-5), particularly in spring/summer, when Northern Hemisphere dust loading peaks (Supplementary Fig. 5). Over reflective regions of North Africa, EMIT leads to enhanced dust warming by more than 4.0 W m^{-2} ; conversely, it predicts stronger cooling over the Middle East. These changes are tightly linked to EMIT-induced changes in iron oxide content (Supplementary Fig. 6) with corresponding impacts upon dust single-scattering albedo (SSA) (Supplementary Fig. 7).

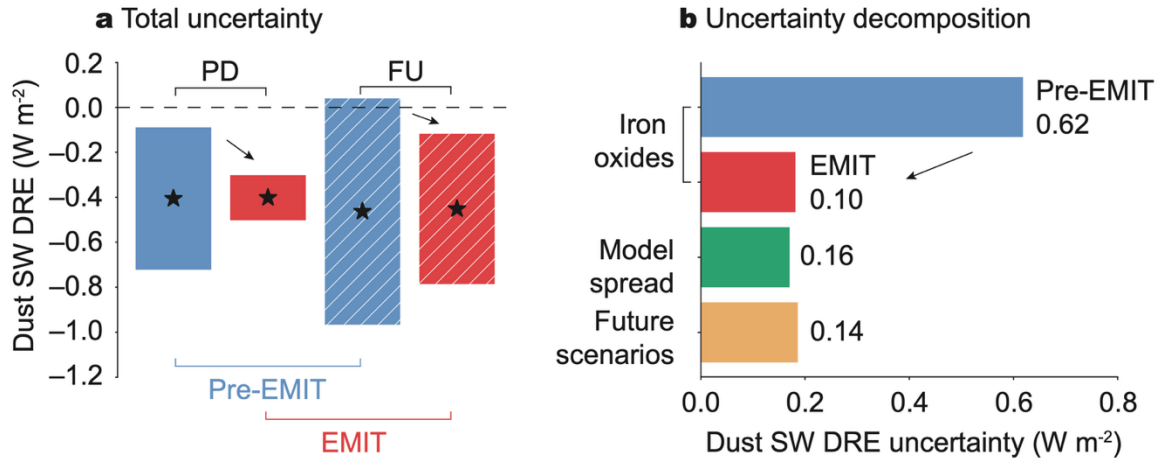


Figure 3. Improved estimates of the dust shortwave (SW) direct radiative effect (DRE). **a**, Ensemble mean (black stars) of global SW DRE at the top of the atmosphere under all-sky conditions in present-day (PD) and future (FU: late 21st century) climates with associated uncertainty (colored bars) for EMIT and pre-EMIT soil mineral atlases. The best estimate is the model ensemble mean; uncertainty reflects dust SW DRE variations from perturbed experiments on key factors such as iron oxide content (irox) and future emission scenarios (Methods). The EMIT uncertainty is significantly lower than the pre-EMIT uncertainty in both the PD and FU climates (one-sided Mann-Whitney U test, p -value < 0.01). **b**, Decomposition of the dust SW DRE uncertainty by individual contributing factors.

Untangling the sources of dust SW DRE spread across experiments

As we delve into understanding the factors that influence the global dust SW DRE, an intriguing picture emerges. Through multiple model analysis, we identify four key drivers that contribute to the dust SW DRE uncertainty, arranged in a clear hierarchy of influence in pre-EMIT simulations (Supplementary Figs. 2, 3, 8): (i) Iron oxide content, (ii) model structural differences, (iii) the contrasting nudged and model winds and their impact upon dust emission and transport, and (iv) emission scenarios derived from shared socioeconomic pathways (SSPs). Among these, iron oxides, represented by the pre-EMIT soil atlases, emerge as the dominant factor (Supplementary Fig. 2). This influence is not a new finding; past studies, both

laboratory experiments^{8,36} and modeling efforts^{7,10}, have highlighted the importance of these minerals to the dust SW DRE. What makes this mineralogical impact particularly striking is its present-day relevance. While the composition of dust remains important for future SW DRE, the magnitude of the future SW DRE is increasingly driven by climate-induced changes in dust emission and transport. Unlike the future, these present-day climate conditions are better constrained by observations, providing a more robust basis for model simulations.

One objective of the EMIT mission was to estimate the dust SW DRE in the future. Despite the common inputs in the ESMs, when examining the future, the models diverge. Both CESM2 and ModelE show similar sensitivity to iron oxide perturbations within observational uncertainties in the present day. However, their projections of the future dust SW DRE differ markedly (Supplementary Fig. 3b), indicating the increasing role of climate-driven factors in shaping dust's radiative impacts on climate.

One of the most significant climate-driven factors is vegetation. Sensitivity experiments using ModelE suggest that future changes to vegetation, especially the response of plants to increased CO₂ levels, account for an additional 20% (pre-EMIT) or 40% (EMIT) of the SW DRE variability (Supplementary Fig. 2). When vegetation is fixed at present-day levels, the model projects stronger global dust cooling (-0.43 W m^{-2}) compared to future scenarios where vegetation is allowed to change dynamically (-0.24 W m^{-2}). The results indicate that CO₂-induced greening (i.e., increased vegetation) could suppress dust emission in certain regions, aligning with earlier findings^{23,24,37}.

The differences between models also contribute to divergent projections of the future dust SW DRE. For example, CESM2 and ModelE yield relatively similar present-day values (-0.41 W m^{-2} and -0.57 W m^{-2} , respectively). However, in future climate scenarios, CESM2 projects stronger dust cooling (-0.56 W m^{-2}) than ModelE (-0.24 W m^{-2}).

EMIT reduces dust SW DRE uncertainties

In the quest to improve the accuracy of the dust SW DRE projections, the EMIT primary mission of detecting surface mineral composition in arid regions plays a pivotal role in reducing uncertainties (Fig. 3). Before the EMIT mineral retrievals were incorporated, uncertainty in the iron oxide content was the dominant factor, accounting for over 90% and 50% of the SW DRE uncertainty estimated using the pre-EMIT soil mineral data in present-day and late-21st-century climates, respectively (Supplementary Fig. 2a). However, with the precise mineral fractions provided by EMIT, this contribution has decreased substantially, dropping to just 20% and 3%, respectively. The impact of the EMIT retrievals is thus profound: it

significantly reduces the SW DRE uncertainty under both present-day and future climate conditions.

Much of the uncertainty reduction is due to iron oxide data provided by EMIT. In pre-EMIT estimates, iron oxide uncertainty alone introduces a 0.62 W m^{-2} impact, over four times greater than that of model spread (0.17 W m^{-2}) in the present day or scenario-related change (0.14 W m^{-2}) (Fig. 3). EMIT reduces this contribution threefold to 0.10 W m^{-2} , bringing it in line with, or even below, other sources of uncertainty. Iron oxides are therefore no longer the dominant uncertainty driver in the global SW DRE estimates (Fig. 3b and Supplementary Fig. 2). This reduction in uncertainty is a crucial step forward in refining our understanding of dust's impact on global climate.

Spatially, EMIT reduces the dust SW DRE uncertainty caused by iron oxide content across most major global dust source regions in the present day, particularly those in the North Africa and Middle East (Fig. 4b). Regional analysis suggests a percentage reduction in uncertainty over 50% for all the nine major sources worldwide in the present day (Fig. 4c). This uncertainty reduction enabled by EMIT remains substantial if all factors are considered in most the major source regions (regional mean reduction still over 50%; Supplementary Fig. 9). The improvement is mainly realized by improved description of iron oxide content compared to that in the pre-EMIT soil mineral atlas (Fig. 1), which consistently indicates that iron oxide content dominates the error sources to the dust SW DRE estimates prior to EMIT.

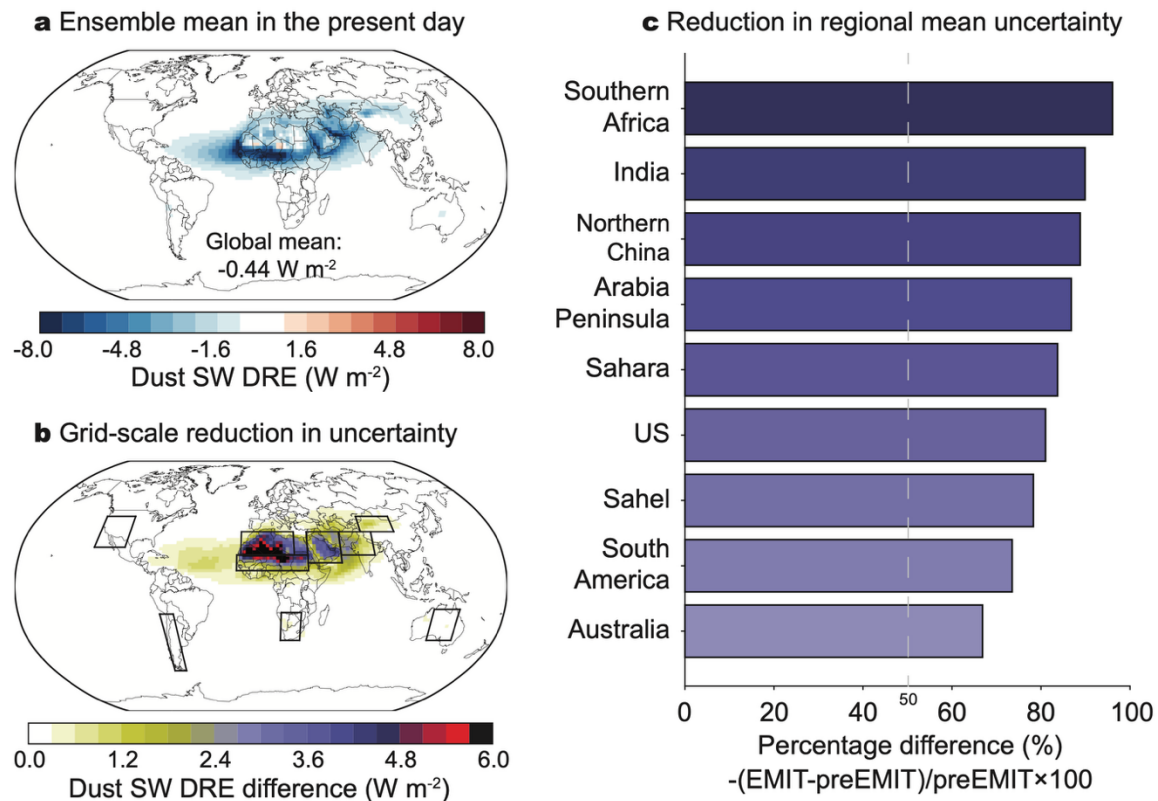


Figure 4. EMIT reduces present-day uncertainty in the shortwave (SW) direct radiative effect (DRE) associated with dust source mineralogy. **a**, Ensemble mean SW DRE from simulations using EMIT soil mineral atlases. **b**, Spatial distribution of the percentage reduction in dust SW DRE uncertainty enabled by EMIT, relative to pre-EMIT soil mineral atlases. **c**, Percentage reduction in regional mean dust SW DRE uncertainty enabled by EMIT, relative to pre-EMIT soil mineral atlases. The uncertainty in the dust SW DRE is primarily governed by the mass fractions of iron oxides, particularly hematite and goethite, with limited sensitivity to the other mineral components⁷. Accordingly, the reduction in the dust SW DRE uncertainty is largely attributable to EMIT's improved characterization of soil iron oxide abundance relative to pre-EMIT mineral atlases.

Future uncertainty projections of the dust SW DRE largely follow present-day patterns (Supplementary Fig. 4). However, the Sahel and oceanic regions downwind of dust sources in North Africa and the Middle East exhibit significantly greater future uncertainty compared to present-day estimates (Supplementary Fig. 9b). This suggests that although EMIT substantially refines present-day estimates, future uncertainties continue to be influenced by various climate factors, including those that are difficult to predict, such as clouds, droughts, and vegetation changes. Nevertheless, EMIT significantly reduces the regional mean uncertainties in the future projections of dust SW DRE across most of the nine major dust source regions (Supplementary Fig. 10).

Despite these gains enabled by EMIT, four pivotal limitations persist. First, the relationship between observed and modeled dust SSA continues to show scatter (Supplementary Fig. 11), even with EMIT's comprehensive global data, pointing to the importance of constraining factors beyond the soil mineral abundances, such as particle size distribution. Second, over oceanic regions (Fig. 4b), EMIT offers only a limited constraint, as the SW DRE here is more sensitive to the other factors such as the size distribution and vertical structure of dust that are subject to model biases³⁸. Third, the LW DRE remains poorly constrained due to the lack of direct detection of quartz and feldspar^{9,10}, which lie beyond EMIT's spectral capabilities, and the absence of their radiative impacts in our models. This partially results in a persistent discrepancy between observed and modeled LW DRE (Supplementary Figure 12). Fourth, the influence of vegetation, which accounts for over 20% of the SW DRE spread across experiments (Supplementary Fig. 2b), exhibits strong model dependence and is uncertain. Our ensemble also underrepresents the full range of potential future climates simulating only the Coupled Model Intercomparison Project Phase 6 (CMIP6) SSP2-4.5 scenario³⁹ in the late-21st-century, underscoring the need for broader sensitivity sampling.

EMIT shifts dust SW DRE research priorities

Our findings recalibrate the research agenda for dust-climate interactions. While

iron oxides remain central to the SW DRE estimate, EMIT's introduction shifts the axis of residual uncertainty. In ESMs using pre-EMIT soil atlases, mineralogy is the primary bottlenecks (Fig. 3 and Supplementary Fig. 2). With EMIT, uncertainty is restructured, now with comparable factors other than soil iron oxides, such as particle size distribution, the influence of vegetation on dust emission and its sensitivity to climate, and the LW DRE of unresolved minerals like quartz and feldspar.

Under warming scenarios, the uncertainty in dust's influence on climate appears to evolve from being dominated by mineral composition to climate-dependent processes. These include uncertainties on processes that shift dust source regions, change vegetation-dust emission sensitivity, and alter dust removal and transport dynamics. These processes are not yet captured by existing ESMs, even though they can represent dust aerosols as component minerals dynamically responsive to climate drivers.

Implications and future directions

The implications of these refined SW DRE estimates are three-fold. First, the narrowed uncertainty around the SW DRE increases the likelihood that dust exerts a non-negligible SW cooling influence in both the present-day and late-21st-century climates. If future dust loading increases in a manner consistent with estimates from the preindustrial era to the late 20th century², it could partially offset greenhouse warming in climate-sensitive regions such as the Sahel and South Asia. In these areas, dust simultaneously affects air quality⁴⁰, ecosystem function⁴¹, and hydrological regimes^{42,43}. Second, EMIT delivers the first observational benchmark for global-scale dust mineral modeling. This benchmark reveals a pivotal transition: uncertainties once dominated by dust mineralogy now likely hinge more on particle size distribution⁴⁴ and processes governing dust emission². Third, EMIT's limited improvement over oceans, where low surface albedo partially covers iron-oxide signals, highlights the urgency of deploying complementary airborne/shipborne campaigns targeting size-resolved dust radiative properties.

Looking forward, three strategic priorities emerge. First, future spaceborne missions should expand mineralogical detection into wavelengths that are sensitive to quartz and feldspar, minerals critical for the dust LW DRE⁹, and cloud ice nucleation in mixed-phase clouds⁴⁵, respectively. These components remain effectively invisible to EMIT but are pivotal for resolving dust's full climate footprint. Second, models should move beyond static mineralogical baselines to incorporate spatial and temporal variations in dust composition. Shifting climate conditions via aridification^{46,47}, CO₂-driven vegetation change²⁴, or cryosphere retreat⁴⁸ may not only alter dust emission but also modify dust sources and thus dust mineral composition, particularly the prevalence of iron oxides. These changes can reshape regional absorption patterns and, by extension, local-to-global climate responses. Third, intensive ground-based campaigns are needed in data-sparse regions to ground-truth orbital retrievals and disentangle mineralogical composition from the

other drivers of the DRE uncertainty. These efforts are equally vital for refining ESMs and informing local dust mitigation strategies, as dust absorption modulates surface heating, atmospheric stability⁴⁹, and even pollutant dispersion⁴⁰.

Beyond radiative impacts, EMIT's mineral atlases unlock entirely new frontiers from snow-darkening feedbacks in cryosphere regions⁵⁰ to iron fertilization in marine biogeochemistry^{5,6}, and to cloud microphysics⁴ influenced by ice-nucleating minerals. With dust mineralogical composition now transformed from a poorly constrained boundary condition into a resolvable Earth system component, this work affirms the transformative potential of orbiting imaging spectroscopy. As ESMs increasingly adopt mineral-resolved representations of dust^{7,25-28}, there is a growing opportunity to better integrate mineralogical detail with dynamical processes to improve our understanding of dust's role in past, present, and future climates.

Methods

The EMIT soil mineral atlases and associated uncertainties

NASA's EMIT mission provides the first high-resolution global atlas of soil mineral mass fractions at 0.5° spatial resolution²⁹. These mass fractions are derived from calibrated VSWIR (visible to shortwave infrared) reflectance spectra collected by the EMIT imaging spectrometer¹⁷ from its position aboard the ISS, using a Hapke-like model in combination with the Tetracorder spectral matching algorithm²⁰.

Key mineral groups, such as chlorite, dolomite, goethite, gypsum, hematite, illite/muscovite, kaolinite, montmorillonite, and vermiculite, are directly mapped, while quartz and feldspar abundances are inferred indirectly due to the absence of diagnostic absorption features in the VSWIR range.

The Supplementary Sections “The state-of-the-art EMIT imaging spectrometer” and “The first high-resolution soil mineral atlases from EMIT and associated uncertainties” respectively describe the EMIT instrument and the methodology used to generate the soil mineral atlases, including the derivation of 95% confidence intervals for mineral mass fractions. Additional details on the spectrometer design and the full methodology for producing the mineral atlases are provided in prior documents¹⁸⁻²⁰. The publicly available EMIT soil mineral atlases are archived at NASA's Distributed Active Archive Center (DAAC)⁵¹ (see “Data availability”). In this study, these publicly available atlases are incorporated into ESMs to derive observationally constrained estimates of the dust SW DRE for both the present day and the late 21st century.

A calibration of a free parameter in the EMIT mineral mass fraction derivation (see Supplementary Section “The first high-resolution soil mineral atlases from EMIT and associated uncertainties”) helps reduce the global bias between modeled and

AERosol RObotic NETwork (AERONET)-based dust SSA compared to pre-EMIT soil mineral atlases (Supplementary Fig. 11). This calibration step ensures consistency between the simulated dust SSA using the retrieved mineralogy and the observed values. However, it limits the use of the AERONET-based dust SSA global bias as an independent validation metric. Consequently, this study emphasizes the reduction in uncertainty enabled by incorporating EMIT-derived soil mineralogy in ESM simulations.

Model descriptions

Three ESMs and one atmospheric chemistry model, which is also referred to as an ESM for brevity, are used in this study: Community Atmosphere Model version 6 (CAM6) embedded within the CESM2, the NASA Goddard Institute for Space Studies (GISS) Earth System ModelE2.1 (referred to as ModelE), the National Oceanic and Atmospheric Administration (NOAA) Geophysical Fluid Dynamics Laboratory (GFDL) AM4, and the Barcelona Supercomputing Center's (BSC) Multiscale Online Nonhydrostatic Atmosphere Chemistry model (MONARCH). All these ESMs were recently enabled to simulate dust aerosol composition as prognostic mineral mixtures^{7,25–28}. The following provides a brief overview of the calculations of dust optical properties and DRE; Supplementary Section “Descriptions of mineral-resolving Earth system models” describes these calculations and each of the four ESMs in detail.

Treatment of optical properties

The four ESMs employ distinct approaches to simulating dust mineralogy, particularly for iron oxides (hematite and goethite), which are critical for modeling dust optical properties in the SW spectrum. Differences among ESMs arise from three key aspects: whether hematite and goethite are distinguished, how mineral mixtures are represented, and the choice of iron oxide refractive indices.

CESM2 and ModelE treat hematite and goethite collectively as a single iron oxide species in their optical property calculations, whereas MONARCH and AM4 distinguish between the two minerals, if both are characterized by a soil atlas. For the mixing state, CESM2 represents iron oxides as part of an internal mixture with all other minerals and aerosol species within each dust mode (i.e., all species presented are internally mixed), both during transport and for radiative calculations. In contrast, ModelE, MONARCH, and AM4 simulate iron oxides in two forms during transport: internally mixed with other minerals and as pure (externally mixed) minerals; for radiative calculations, however, they are treated as internally mixed with a host mixture composed of the other (weakly absorbing) minerals. For further details on each model, see Supplementary Section “Descriptions of mineral-resolving Earth system models”.

As to refractive indices of individual minerals, all models use identical data sourced from the same prior study²⁷ for non-iron-oxide minerals. For iron oxides, although

the refractive indices in the SW spectrum differ slightly between CESM2 and the other three models, these differences are relatively minor^{31,32}; moreover, the variables related to the dust SW DRE simulated by all the four ESMs are reasonably consistent with retrievals of satellite-based SW DREE at the top of the atmosphere under clear-sky conditions and AERONET-based mid-visible-band (0.44-0.63 μm) SSA (Supplementary Figure 11).

CESM2 uses the Modal Aerosol Module (MAM4) with three dust modes, while the other three models simulate dust with a binned method. Aerosol optical properties in CESM2 are calculated based on the wet surface mode radius and wet refractive index of each component, with hygroscopic growth estimated using κ -Köhler theory⁵². CESM2 applies the volume mixing rule to derive the refractive indices of the mixture and parameterizes optical properties using Chebyshev polynomials⁵². This approach captures the effects of composition, size, and ambient humidity on the aerosol optical property diagnostics. Because of the use of the parameterized optical properties, CESM2 simulates SSA collectively for all aerosols rather than dust alone; dust-specific values are estimated by selecting pixels where dust contributes more than 50% of the total aerosol optical depth in the mid-visible band (0.44-0.63 μm). In contrast, the other models directly simulate SSA for dust aerosols (Supplementary Section “Descriptions of mineral-resolving Earth system models”).

Diagnostics of dust DRE and DREE

In each of the four ESMs, the dust DRE is diagnosed as the difference in net radiative fluxes with and without dust aerosols, computed for both SW and LW bands. The simulated dust DREE is evaluated against clear-sky observations at the top of the atmosphere. Robust inter-model and model-observation comparisons are complicated by methodological heterogeneity in diagnosing clear-sky DRE across the four ESMs and by sampling limitations specific to ModelE. Accordingly, the analysis relies on all-sky DRE values for ModelE and for models (i.e., MONARCH and AM4), where clear-sky DRE was not explicitly archived. This likely has little impact on the model-observation comparisons over the key dust source region, the Sahara Desert, where low cloud cover means that the difference of clear-sky and all-sky DRE values is not substantial.

ESM simulations

We conducted 36 ESM simulations using both pre-EMIT and EMIT soil mineral atlases as inputs for the four ESMs (see Supplementary Section “Descriptions of mineral-resolving Earth system models” for model configurations).

We focus on the dust SW DRE, because EMIT’s contributions to reducing the dust DRE are not uniform across all spectral bands or geographic domains. Over oceanic regions, improvements resulting from EMIT constraints upon dust mineral composition are limited (Figs. 2, 4), due to the greater sensitivity of the SW DRE to factors like dust size and concentrations that result from transport biases³⁸.

Similarly, the LW DREE remains largely unaffected (Supplementary Fig. 12), as EMIT does not retrieve the soil fractions of key absorptive minerals at thermal wavelengths, such as quartz^{7,9,10}, which lack prominent spectral signatures in the wavelength range measured by EMIT. Instead, the mass fractions of quartz and feldspar are inferred from the Hapke-like model using grain size retrieved from EMIT reflectance²⁰ (see Supplementary Section “The first high-resolution soil mineral atlases from EMIT and associated uncertainties”). The partitioning of these minerals into clay and silt fractions is subsequently derived from the empirical relationships presented in C1999, applied to the soil texture retrieved from each EMIT scene²⁰.

The dust SW DRE is strongly influenced by the mineral fraction of iron oxides such as hematite and goethite^{7,10,53}. We incorporate best estimates and 95% confidence intervals for iron oxides from the pre-EMIT and EMIT atlases. These simulations capture key drivers of the simulated DRE, including emission scenarios, vegetation and drought variability, and model-specific sensitivities to the atmospheric circulation.

Supplementary Tables 1-2 summarize the numerical experiments conducted in this study, which form the basis for quantifying the dust SW DRE and its associated uncertainty under present-day and late-21st-century climate conditions. The following three subsections provide detailed descriptions of these experiments.

Present-day dust SW DRE using EMIT

The dust aerosol burden or load is intimately related to meteorological processes like winds that raise and transport dust particles. We attempt to match the model winds to those observed by relaxing toward reanalysis values from the Modern-Era Retrospective analysis for Research and Applications dynamics version 2 (MERRA2) or else the National Centers for Environmental Prediction (NCEP) or European Centre for Medium-Range Weather Forecasts (ECMWF) Reanalysis version 5 (ERA5). We use reanalysis values between 2006 and 2011. This period is chosen to allow comparison to previous sensitivity studies⁷ along with observations. Sea surface temperature and sea ice are prescribed from observations during this period. During the first year (2006), the dust cycle “spins up” to statistical equilibrium and is excluded from the data analysis. These experiments, denoted as “(ESM name)-(mineral atlas)_base_(reanalysis product)” in Supplementary Table 1, are our best estimate of the present-day dust DRE.

Additional experiments simulating the present-day dust cycle are carried out to estimate the uncertainty of our best estimate DRE. These experiments are also listed in Supplementary Table 1. Previous work demonstrates that the soil mass fraction of hematite and goethite makes the largest contribution to the DRE uncertainty⁷ in mineral-resolved ESMs. To bound the SW DRE uncertainty, we carry out two types of experiments (e.g., “EMIT_hi_iron” and “EMIT_low_iron”) using the EMIT soil mineral atlases, perturbing the hematite and goethite soil fractions to their

respective retrieved high and low values, based upon the uncertainty of the quartz-feldspar grainsize parameter (see Section “The first high-resolution soil mineral atlases from EMIT and associated uncertainties”).

In the absence of meteorological reanalysis to drive calculations of future DRE in the late 21st century, we use winds computed prognostically by CESM2 and ModelE. For comparison of present-day and future control experiments, we add present-day experiments “freeWD”, where the dust DRE is calculated with prognostic winds.

Uncertainty in present-day dust SW DRE before EMIT

To assess the effect of EMIT retrievals of soil composition compared to previous estimates by pre-EMIT soil mineral atlases, we estimate the SW DRE in two additional types of experiments using these prior estimates of soil minerals (Supplementary Table 1: “C1999” and “J2014”).

Prior to EMIT, spatial variations in soil mineral composition were inferred through a global atlas that compiled observations of regionally varying soil descriptors like soil type¹⁴ or soil unit¹⁵. Each type or unit was assumed to have a characteristic fractional distribution of minerals that was identical at every location where that descriptor was indicated by the atlas. This assumption was necessitated by the extremely limited number of direct measurements of soil mineral composition. Uncertainty of soil mineral fractions thus arose through two effects: the uncertain characteristic mineral fractions for each soil descriptor that were inferred empirically through limited measurements, and uncertainty in the gridded soil descriptor provided by the atlas that was constructed from multiple regional surveys with spatially inhomogeneous sampling density and especially low resolution in the remote arid regions that are prolific dust sources.

DRE uncertainty prior to the availability of EMIT mineral composition retrievals was estimated by a previous study⁷ using a wide range of sensitivity studies with CESM2, as well as complementary experiments with ModelE, AM4, and MONARCH. These experiments focused on the DRE uncertainty due to poorly constrained knowledge of soil minerals before EMIT. Two different atlases prescribing the mineral content of soils were used (C1999 and J2014). Based on the reported soil mineral ranges¹⁴, the previous study⁷ calculated the 95% confidence interval of iron oxides for each soil type. The DREs were then calculated in sensitivity studies based on the high and low distribution of mineral content in the soils⁷. Their analysis⁷ showed that the SW DRE uncertainty is most dependent on the hematite and goethite mass fractions, with little dependence upon other mineral fractions, especially those not detected by EMIT (i.e., quartz and feldspar). Overall, the range of dust net DRE was calculated to be -0.23 to 0.35 W m⁻², and over 90% of this uncertainty is due to uncertainty in the soil mineralogy⁷. Smaller uncertainty results from different estimates of aerosol mineral composition by different models (despite using the same soil mineral atlas).

These calculations characterize the uncertainty related to the mineral fractions that

are attributed to each soil type or unit, and which are derived based upon limited measurements. This underestimates the true mineral uncertainty by excluding contributions from the mischaracterization of soil type or unit within the atlas at any location due to limited spatial sampling and uncertain interpolation. To account for this “unknown” uncertainty caused by limited measurements based on which the pre-EMIT soil mineral atlases were created and by the challenges in quantifying uncertainty in the soil type atlas used to infer mineral composition, we consider the difference between C1999 and J2014 base simulations as an error source of iron oxides.

Future projections of dust, SW DRE, and associated uncertainties

Future experiments take atmospheric composition (including CO₂ and concentrations of non-dust aerosol species) and ocean surface conditions (including sea surface temperature and sea ice) from coupled experiments that are part of the standard CMIP6 protocol, carried out separately with CESM2 and ModelE. Here we estimate the dust SW DRE, using EMIT soil atlases and the mineral-resolved version of each model, allowing changes to the present-day source extent due to projected vegetation changes.

In order to quantify the future dust SW DRE, as a result of changes in dust source area from climate change, CESM2 and ModelE are run with prognostic winds and the best estimate of the EMIT soil mineral atlas to simulate future climate in the late 21st century, 2090-2094: experiments denoted by “Future_BASE” in Supplementary Table 2. To diagnose future changes in the SW DRE, based on the EMIT soil atlases, this set of simulation is contrasted to the “Present-day_online” experiment in Supplementary Table 1. As with the present-day experiments, we include simulations spanning the uncertainty range of soil mass fractions of hematite and goethite retrieved by EMIT, denoted by “hi_iron_FU” and “low_iron_FU”, respectively. Separate experiments show the effect of EMIT retrievals compared to using prior soil mineral atlases, denoted by “C1999_base_FU” and “J2014_base_FU”.

Uncertainty of future dust DRE is characterized using different scenarios, as projected by CESM2 and ModelE, to at least partially cover the spread among late-21st-century climate projections by CMIP6. A key uncertainty of future DRE projections results from uncertain projections of vegetation. Previous studies suggest that most models predict an increase in leaf area index coverage in the future⁵⁴, indicating a likely decrease in dust source regions, although this is sensitive to the assumptions of CO₂ fertilization³⁷. CESM2 calculates vegetation prognostically, whereas vegetation is prescribed in ModelE. For the standard “base_FU” scenario, ModelE uses the leaf area index from CESM2. To see the effect of leaf area index changes upon dust DRE over the late 21st century, we carry out two additional experiments with 2090-2094 atmospheric composition and present-day or future vegetation (denoted in Supplementary Table 2 by “ModelE_CAMvegPD” and “ModelE_CAMvegFU”, respectively).

Finally, we consider the sensitivity of the dust SW DRE to late-21st-century atmospheric composition according to the CMIP6 intermediate-mitigation (SSP2-4.5) and high-emissions (SSP5-8.5) scenarios, using CESM2 whose vegetation responds prognostically to this range of dust DRE (“base_FU245” and “base_FU585”, respectively, in Supplement Table 2). Although fully characterizing the influence of future climate uncertainty is beyond the scope of the EMIT mission, differences among the ESMs with varying climate sensitivities offer some insight into the range of dust-climate interactions in a warming world.

Recognizing that some ESMs simulate a relatively flat dust trend from the pre-industrial era to the year 2000, which contrasts with the $\sim 55\%$ increase according to deposition measurements², we conducted an additional experiment to evaluate the implications of this alternative trend on future projections. In this experiment, we increased dust optical depth in the mid-visible band by $\sim 30\%$, extrapolating the rate since the pre-industrial suggested by dust proxies². This amplifies the dust SW DRE to -0.57 W m^{-2} with the EMIT soil mineral atlas and -0.51 W m^{-2} with the pre-EMIT atlases.

Quantifying uncertainty in dust SW DRE

We divide the factors affecting the dust SW DRE (ξ) estimate into four subcategories: dust mineral composition, assumed to be dominated by the mass fraction of iron oxides (φ), model spread (σ), future scenarios (ψ), and vegetation dynamics (η). The iron oxide fraction is assumed to dominate the compositional uncertainty ($\Delta\xi$) in the dust SW DRE based upon a prior study⁷. We perturb the iron oxide abundance based on the best estimates described in both EMIT (E) and C1999 (C) or J2014 (J) soil mineral atlases (Q). The resultant high- ($\Delta\xi_{Q_h}$) or low-branch ($\Delta\xi_{Q_l}$) uncertainty is obtained by calculating the difference between the SW DRE from the base mineral simulation and that from the paired uncertainty experiments in each model (m) with either increased (φ_{Q_h}) or decreased (φ_{Q_l}) iron oxide fractions.

We first determine whether the dust SW DRE in a perturbed experiment represents more cooling or warming compared to the base (b) simulation. We then calculate the uncertainty for each branch by finding the difference between the simulated dust SW DRE from the paired simulations in each ESM using the EMIT or C1999 soil mineral atlases. For example, when using the EMIT (E) soil atlas, the high-branch uncertainty in the dust SW DRE, $\Delta\xi(\varphi_{E_h,m})$ with respect to the best estimate of the dust SW DRE, $\xi(\widetilde{\varphi_{E_b,m}})$ in model m (i.e., CESM2 and ModelE) due to higher (h) soil iron oxides (φ_{E_h}) relative to the base value ($\widetilde{\varphi_{E_b,m}}$), is calculated as follows:

$$\Delta\xi(\varphi_{E,m})_h = \left| \xi(\varphi_{E_h,m}) - \xi(\widetilde{\varphi_{E_b,m}}) \right|. \quad (1)$$

There are multiple paired simulations in CESM2 with C1999, which has two

simulations representing high-bound iron oxides, one for iron oxides in the clay-sized category (c) and the other for those in the silt-sized category (s). Although each simulation isolates perturbations in a single dust size category, both contribute similarly to the dust SW DRE due to their shared dust source regions, emission processes, and percentage uncertainties. Therefore, we calculate their sum to represent the amplitude for this high branch:

$$\Delta\xi(\varphi_{c,m})_h = \left| (\varphi_{c_{hc},m}) - \xi(\widetilde{\varphi_{c_b,m}}) \right| + \left| \xi(\varphi_{c_{hs},m}) - \xi(\widetilde{\varphi_{c_b,m}}) \right|, \quad (2)$$

where m refers specifically to CESM2.

The low-branch dust SW DRE uncertainty, $\Delta\xi(\varphi_{q,m})_l$ with respect to the best estimate of the dust SW DRE in model m due to lower (l) soil iron oxides relative to the base value using the pre-EMIT or EMIT soil atlases, is calculated using the same approach.

The uncertainty resulting from the pre-EMIT soil atlases is harder to quantify because the soil mineral fractions are inferred indirectly from other observed quantities following multiple assumptions. In the absence of global measurements of soil minerals prior to EMIT, the mineral fractions were derived from a soil descriptor like soil type (C1999) that was available from a global atlas. Each soil type is assumed to have a characteristic mineral composition based upon empirical relations derived from the limited number of soil measurements. Thus, the total uncertainty has a contribution from the imprecise relation between soil type and composition. This is the first term in Equation (3) below. Additional uncertainty results from the use of two alternative soil descriptors to infer the mineral fractions: soil type (C1999) or soil unit (J2014). Thus, our estimate of the pre-EMIT (P) high-branch uncertainty $\Delta\xi(\varphi_{p,m})_h$ additionally includes the magnitude of the difference between C1999 (C) and J2014 (J) as an error source to account for the differing base values of the dust SW DRE resulting from whether soil type or unit is chosen to specify the iron oxide fraction:

$$\Delta\xi(\varphi_{p,m})_h = \sqrt{\left(\Delta\xi(\varphi_{c,m})_h\right)^2 + \left[\xi(\widetilde{\varphi_{j_b,m}}) - \xi(\widetilde{\varphi_{c_b,m}})\right]^2}. \quad (3)$$

The two terms in this Equation (3) represent distinct and uncorrelated sources of uncertainty: one captures variability within a single mineral atlas (Gaussian spread), while the other reflects systematic bias between different soil mineral atlases (mean difference).

There is an additional contribution to pre-EMIT uncertainty that is harder to quantify that results from misidentification in the global atlas of the soil descriptor at a particular location where the descriptor was derived by interpolation rather than direct observation. The global atlas is constructed from interpolation of

measurements made with varying spatial resolution that are often concentrated in agricultural regions rather than arid dust sources. This contribution to uncertainty and its spatial variation is difficult to reconstruct; we simply note its existence, while omitting it, and regard Equation (3) as a conservative estimate of the total pre-EMIT uncertainty. Note that this contribution from interpolation, along with the final term in Equation (3), are absent in the EMIT uncertainty, because EMIT provides direct retrievals of mineral composition at each location where dust is emitted.

If the same paired simulations exist in other ESMs like ModelE, we repeat the calculation for each branch and then average the obtained results across different models with a soil mineral atlas Q :

$$\overline{\Delta\xi(\varphi_Q)_h} = \frac{1}{N_{model}} \sum_{m=1}^{N_{model}} \Delta\xi(\varphi_{Q,m})_h. \quad (4)$$

This approach assumes that the response to the perturbed parameter in the different ESMs is correlated: for example, increased iron oxides in the soil compared to the baseline simulation causes more warming in all the ESMs.

The half-length uncertainty in the dust SW DRE due to iron oxides is calculated as follows, ensuring a symmetric uncertainty centered about the base best result:

$$\Delta\xi(\overline{\varphi_Q}) = \max_{o=h,l} \overline{\Delta\xi(\varphi_Q)_o}. \quad (5)$$

The total 95% confidence interval is subsequently derived based on the model ensemble mean of the best estimates of the dust SW DREs, $\xi(\overline{\varphi_Q})$, across simulations using the base soil mineral atlases, and $\Delta\xi(\overline{\varphi_Q})$:

$$95\%CI_Q = [\xi(\overline{\varphi_Q}) - \Delta\xi(\overline{\varphi_Q}), \xi(\overline{\varphi_Q}) + \Delta\xi(\overline{\varphi_Q})]. \quad (6)$$

Model spread (σ) in simulating the dust SW DRE is quantified as the standard deviation (σ_{std}) of the SW DRE values simulated by all the ESMs:

$$\sigma = 1.96\sigma_{std}. \quad (7)$$

We also treat differences caused by the use of prognostic versus reanalyzed winds within the same model as a type of model spread.

Similarly, we calculate the dust SW DRE difference, ψ and η , arising from different emission scenarios in future simulations, if projection uncertainty is considered, and from vegetation dynamics, respectively.

To combine these factors, we assume that each factor (iron oxides, emission scenarios, vegetation, and model spread) is independent of the others and used a root mean square sum of the uncertainties caused by each factor in the paired models with a total model number of N_σ , N_ψ , and N_η , respectively:

$$\Delta\xi(Q) = \sqrt{\Delta\xi(\varphi_Q)^2 + \sigma^2/N_\sigma + \psi^2/N_\psi + \eta^2/N_\eta}. \quad (8)$$

Uncertainty in the present-day and late 21st-century dust SW DRE is quantified using the same methodology described above, applied to simulations for each respective period. A combined estimate of uncertainty across both time periods is also derived, incorporating all simulations used to assess the relative importance of contributing factors to dust SW DRE variability.

Quantifying uncertainty in soil and airborne iron oxides

The uncertainty in the model-simulated change in airborne iron oxide mass fractions ($\Delta\varphi_Q$), based on either EMIT (P) or pre-EMIT (E) soil mineral atlases, is calculated using the same procedure outlined in Equations (1-6), substituting the dust SW DRE with the iron oxide mass fraction. The relative reduction in uncertainty (ε) provided by EMIT, compared to pre-EMIT soil mineral atlases, is then computed as follows and shown in Fig. 1a:

$$\varepsilon = -100(\Delta\varphi_P - \Delta\varphi_E)/\Delta\varphi_P. \quad (9)$$

For soil iron oxides, differences across models are minimal, as all use the same underlying soil mineral atlas. The uncertainties for both EMIT and pre-EMIT atlases are derived directly from the best estimates and associated 95% confidence intervals reported by each product. We then calculate probability distributions across 16 bins, each spanning 5%, from 20% to 100% iron oxide mass fraction, and present the results in Fig. 1b.

Observational dust SSA

We derive climatological means of observed dust SSA in the mid-visible band (0.44-0.63 μm) from AERONET Version 3 Level 2.0 Almucantar retrievals for total aerosols^{55,56}. To isolate dust-dominated conditions, we apply stringent filters:

1. Fine-mode exclusion: Removing retrievals with a fine-mode aerosol volume fraction larger than 10% minimizes contamination from non-dust fine-sized aerosol species (e.g., sulfate, nitrate, and organics, including absorbing carbonaceous aerosols like black/brown carbon).
2. SSA spectral signature: Retaining only retrievals where SSA increases from 0.440 to 0.675 μm distinguishes dust from all other aerosols, including sea salt which exhibits a spectrally flat SSA⁵⁷.
3. Absorption threshold: Excluding data with an imaginary refractive index larger than 0.004286 (averaged over 0.675-1.02 μm)⁵⁸ further reduces carbonaceous aerosol interference.

These criteria are applied to hourly data during the 2007-2011 period. Monthly dust SSA is computed as an extinction-weighted mean, considering only months with more than 80 hourly measurements over the 5-year period. While this approach improves the prominence and fidelity of the dust signal, residual non-dust contamination remains difficult to quantify.

Observational dust DREE

Observational data of the clear-sky SW and LW DREE at the top of the atmosphere, as summarized in Supplementary Tables 3 and 4, respectively, are used to evaluate model performance. The observational DREE were derived in previous studies from space-borne or ground-based observations and, in some cases, including 1-D radiative transfer modeling. While there are observations of surface clear-sky DREE, our study focuses exclusively on those at the top of the atmosphere.

Most observational estimates are for daytime, while model results represent monthly fully diurnal averages. For a consistent comparison, daytime observations are converted to fully diurnal averages by accounting for the day-night duration during the observation months and assuming zero SW DREE at night. Given the diurnal cycle of the LW DREE, which peaks during the day and remains nonzero at night, a correction is applied to convert daytime estimates to diurnal averages, which are approximately 80% of the original values⁵⁹.

Acknowledgments

LL, NMM, RLM, BLE, and RNC received support from the NASA EMIT project. EMIT is supported by the NASA Earth Venture Instrument program under the Earth Science Division of the Science Mission Directorate. LL and NMM also acknowledge assistance from Department of Energy (DOE) DE-SC0021302, and the high-performance computing resources from Derecho provided by NCAR's Computational and Information Systems Laboratory (CISL), sponsored by the National Science Foundation. RLM also received support from the NASA Modeling, Analysis and Prediction Program. CPGP, MGA, BLE, and VO acknowledge funding by the European Research Council under the Horizon 2020 research and innovation programme through the ERC Consolidator Grant FRAGMENT (grant agreement No.

773051), Spanish Ministerio de Economía y Competitividad through the HEAVY (grant no. PID2022-140365OB-I00) and BIOTA (PID2022-139362OB-I00) projects funded by MCIN/AEI/10.13039/501100011033 and by ERDF/EU), the AXA Research Fund through the AXA Chair on Sand and Dust Storms at BSC, and the European Union's Horizon 2020 research and innovation programme under grant agreements No 821205 (FORCeS) and No 101137680 (CERTAINTY). A portion of this research was performed at the Jet Propulsion Laboratory, California Institute of Technology, under a contract with NASA. We thank Raymond F. Kokaly, Gregg A. Swayze, Francisco Ochoa, and Abigail Keebler for their contributions to the generation of the EMIT soil mineral atlases.

Competing interests

The authors declare no competing interests.

Contributions

L.L. and N.M.M. conceived the study and designed the modeling experiments. L.L. performed the CESM2 simulations (18 in total), carried out the analysis (including results from all the four models), and drafted the initial manuscript. L.L. and N.M.M. co-wrote the experiment design section. R.L.M. contributed to the experimental design, performed the ModelE simulations (13 in total), processed the model results, and provided the description of the ModelE model. C.P.G.-P. and M.G.A. also contributed to the experimental design. V.O. performed the MONARCH simulations (2 in total) and the comparison between models and AERONET dust SSA. M.G.A. processed AERONET data to create the climatological monthly means of dust SSA used in the comparison. V.O. and M.G.A. provided the description of the MONARCH model. P.G. conducted the AM4 simulations (3 in total) and processed the model results. Q.S. and P.G. wrote the description of the AM4 model. D.R.T. wrote the description of the EMIT instrument. P.G.B., M.G.A., R.L.M., C.P.G.-P., and L.L. authored the description of the EMIT soil mineral atlas sections. All remaining authors, along with those previously mentioned, contributed to the generation of the EMIT soil mineral atlases. R.O.G. is the principal investigator of the EMIT project. All authors contributed to editing the manuscript.

Data availability

The data presented in Figs. 1-4 are available at <https://doi.org/xxxxx>.

Code availability

The codes to carry out the analyses are available upon request from the primary corresponding author, Longlei Li.

References

1. Kok, J. F. *et al.* Contribution of the world's main dust source regions to the global cycle of desert dust. *Atmos Chem Phys* **21**, 8169–8193 (2021).
2. Kok, J. F. *et al.* Mineral dust aerosol impacts on global climate and climate change. *Nat Rev Earth Environ* (2023) doi:10.1038/s43017-022-00379-5.
3. Sokolik, I. N. & Toon, O. B. Direct radiative forcing by anthropogenic airborne mineral aerosols. *Nature* **381**, 681–683 (1996).
4. DeMott, P. J. *et al.* African dust aerosols as atmospheric ice nuclei. *Geophys Res Lett* **30**, 1732, doi:10.1029/2003GL017410, 2003 (2003).
5. Mahowald, N. M. *et al.* Atmospheric global dust cycle and iron inputs to the ocean. *Global Biogeochem Cycles* **19**, GB4025 (2005).
6. Jickells, T. D. *et al.* Global iron connections between desert dust, ocean biogeochemistry, and climate. *Science* (1979) **308**, (2005).
7. Li, L. *et al.* Quantifying the range of the dust direct radiative effect due to source mineralogy uncertainty. *Atmos Chem Phys* **21**, 3973–4005 (2021).
8. Lafon, S., Sokolik, I. N., Rajot, J. L., Caquinau, S. & Gaudichet, A. Characterization of iron oxides in mineral dust aerosols: Implications for light absorption. *Journal of Geophysical Research Atmospheres* **111**, 1–19 (2006).
9. Sokolik, I. N. & Toon, O. B. Incorporation of mineralogical composition into models of the radiative properties of mineral aerosol from UV to IR wavelengths. *Journal of Geophysical Research Atmospheres* **104**, 9423–9444 (1999).
10. Li, L. & Sokolik, I. N. The Dust Direct Radiative Impact and Its Sensitivity to the Land Surface State and Key Minerals in the WRF-Chem-DuMo Model: A Case Study of Dust Storms in Central Asia. *Journal of Geophysical Research: Atmospheres* **123**, 4564–4582 (2018).
11. Tang, I. N. Chemical and size effects of hygroscopic aerosols on light scattering coefficients. *Journal of Geophysical Research Atmospheres* **101**, 19245–19250 (1996).
12. Dufresne, J. L., Gautier, C. & Ricchiazzi, P. Longwave scattering effects of mineral aerosols. *J Atmos Sci* **59**, 1959–1966 (2002).
13. Liao, H. & Seinfeld, J. H. Radiative forcing by mineral dust aerosols: Sensitivity to key variables. *Journal of Geophysical Research Atmospheres* **103**, 31637–31645 (1998).
14. Claquin, T., Schulz, M. & Balkanski, Y. Modeling the mineralogy of atmospheric dust sources. *J Geophys Res* **104**, 22,222–243,256 (1999).
15. Journet, E., Balkanski, Y. & Harrison, S. A new data set of soil mineralogy for dust-cycle modeling. *Atmos Chem Phys* **14**, 2014–3801 (2014).
16. Green, R. O. *et al.* The Earth Surface Mineral Dust Source Investigation: An Earth Science Imaging Spectroscopy Mission. *IEEE Aerospace Conference Proceedings* (2020) doi:10.1109/AERO47225.2020.9172731.
17. Thompson, D. R. *et al.* On-orbit calibration and performance of the EMIT imaging spectrometer. *Remote Sens Environ* **303**, (2024).
18. Okin, G. S. *et al.* *EMIT L3 Algorithm: Aggregated Mineral Spectral Abundance Theoretical Basis*. (2023).
19. Brodrick, P. G. *et al.* *Earth Surface Mineral Dust Source Investigation (EMIT) EMIT L2b Algorithm: Mineral Detection and Related Products at the Pixel Scale Theoretical Basis*. (2023).

20. Clark, R. N. *et al.* Imaging Spectroscopy: Earth and Planetary Remote Sensing with the PSI Tetracorder and Expert Systems from Rovers to EMIT and Beyond. *Planetary Science Journal* **5**, (2024).
21. Mahowald, N. *et al.* *EMIT L4 Algorithm: Earth System Model Products Theoretical Basis*. (2024).
22. Brodrick, P. *et al.* The Earth Surface Mineral Dust Source Investigation (EMIT): Global Distributions of Mineralogy in Arid Lands. in 11–15 (American Geophysical Union Fall Meeting, San Francisco, CA, 2023). doi:GC53B-05.
23. Mahowald, N. M. & Luo, C. A less dusty future? *Geophys Res Lett* **30**, (2003).
24. Mahowald, N. M. *et al.* Climate response and radiative forcing from mineral aerosols during the last glacial maximum, pre-industrial, current and doubled-carbon dioxide climates. *Geophys Res Lett* **33**, (2006).
25. Li, L. *et al.* Importance of different parameterization changes for the updated dust cycle modeling in the Community Atmosphere Model (version 6.1). *Geosci Model Dev* **15**, 8181–8219 (2022).
26. Perlwitz, J. P., Pérez García-Pando, C. & Miller, R. L. Predicting the mineral composition of dust aerosols - Part 1: Representing key processes. *Atmos Chem Phys* **15**, 11593–11627 (2015).
27. Scanza, R. A. *et al.* Modeling dust as component minerals in the Community Atmosphere Model: Development of framework and impact on radiative forcing. *Atmos Chem Phys* **15**, (2015).
28. Gonçalves Ageitos, M. *et al.* Modeling dust mineralogical composition: sensitivity to soil mineralogy atlases and their expected climate impacts. *Atmos Chem Phys* **23**, 8623–8657 (2023).
29. Green, R. EMIT L3 Aggregated Mineral Spectral Abundance and Uncertainty 0.5 Deg V001. <https://doi.org/10.5067/EMIT/EMITL3ASA.001> (2023) doi:<https://doi.org/10.5067/EMIT/EMITL3ASA.001>.
30. Kok, J. F., Ward, D. S., Mahowald, N. M. & Evan, A. T. Global and regional importance of the direct dust-climate feedback. *Nat Commun* **9**, (2018).
31. Li, L. *et al.* Improved constraints on hematite refractive index for estimating climatic effects of dust aerosols. *Commun Earth Environ* **5**, (2024).
32. Obiso, V. *et al.* Observationally constrained regional variations of shortwave absorption by iron oxides emphasize the cooling effect of dust. *Atmos Chem Phys* **24**, 5337–5367 (2024).
33. Coleman, R. W. *et al.* An accuracy assessment of the surface reflectance product from the EMIT imaging spectrometer. *Remote Sens Environ* **315**, 114450 (2024).
34. Sand, M. *et al.* Aerosol absorption in global models from AeroCom phase III. *Atmos Chem Phys* **21**, 15929–15947 (2021).
35. Kok, J. F. *et al.* Smaller desert dust cooling effect estimated from analysis of dust size and abundance. *Nat Geosci* **10**, 274–278 (2017).
36. Di Biagio, C. *et al.* Complex refractive indices and single-scattering albedo of global dust aerosols in the shortwave spectrum and relationship to size and iron content. *Atmos Chem Phys* **19**, 15503–15531 (2019).
37. Mahowald, N. M. Anthropocene changes in desert area: Sensitivity to climate model predictions. *Geophys Res Lett* **34**, (2007).

38. Meng, J. *et al.* Improved Parameterization for the Size Distribution of Emitted Dust Aerosols Reduces Model Underestimation of Super Coarse Dust. *Geophys Res Lett* **49**, 1–12 (2022).
39. Tebaldi, C. *et al.* Climate model projections from the Scenario Model Intercomparison Project (ScenarioMIP) of CMIP6. *Earth System Dynamics* **12**, 253–293 (2021).
40. Prospero, J. M., Collard, F. X., Molinié, J. & Jeannot, A. Characterizing the annual cycle of African dust transport to the Caribbean Basin and South America and its impact on the environment and air quality. *Global Biogeochem Cycles* **28**, 757–773 (2014).
41. McTainsh, G. & Strong, C. The role of aeolian dust in ecosystems. *Geomorphology* **89**, 39–54 (2007).
42. Miller, R. L., Tegen, I. & Perlwitz, J. Surface radiative forcing by soil dust aerosols and the hydrologic cycle. *Journal of Geophysical Research: Atmospheres* **109**, (2004).
43. Miller, R. L., Knippertz, P., Pérez García-Pando, C., Perlwitz, J. P. & Tegen, I. Impact of dust radiative forcing upon climate. in *Mineral Dust: A Key Player in the Earth System* (eds. Knippertz, P. & Stuut, J. B. W.) 327–357 (Springer, Dordrecht, 2014). doi:10.1007/978-94-017-8978-3_13.
44. Mahowald, N. M. *et al.* The size distribution of desert dust aerosols and its impact on the Earth system. *Aeolian Res* **15**, (2014).
45. Atkinson, J. D. *et al.* The importance of feldspar for ice nucleation by mineral dust in mixed-phase clouds. *Nature* **498**, 355–358 (2013).
46. Prospero, J. M. & Lamb, P. J. African Droughts and Dust Transport to the Caribbean: Climate Change Implications. *Science (1979)* **32**, 1024–1027 (2003).
47. Middleton, N. J. Effect of drought on dust production in the Sahel. *Nature* **316**, 431–434 (1985).
48. Bullard, J. E. Contemporary glacial inputs to the dust cycle. *Earth Surf Process Landf* **38**, 71–89 (2013).
49. Pérez, C., Nickovic, S., Pejanovic, G., Baldasano, J. M. & Özsoy, E. Interactive dust-radiation modeling: A step to improve weather forecasts. *Journal of Geophysical Research Atmospheres* **111**, D16206 (2006).
50. Skiles, S. M. K., Flanner, M., Cook, J. M., Dumont, M. & Painter, T. H. Radiative forcing by light-absorbing particles in snow. *Nat Clim Chang* **8**, 964–971 (2018).
51. Brodrick, P. , *et al.* EMIT L3 Aggregated Mineral Spectral Abundance and Uncertainty 0.5 Deg V001 [Data set]. *NASA Land Processes Distributed Active Archive Center* (2023) doi:https://doi.org/10.5067/EMIT/EMITL3ASA.001.
52. Ghan, S. J. & Zaveri, R. A. Parameterization of optical properties for hydrated internally mixed aerosol. *Journal of Geophysical Research Atmospheres* **112**, 1–10 (2007).
53. Moosmüller, H. *et al.* Single scattering albedo of fine mineral dust aerosols controlled by iron concentration. *J Geophys Res* **2006**, 2004–2008 (2012).
54. Mahowald, N. *et al.* Projections of leaf area index in earth system models. *Earth System Dynamics* **7**, 211–229 (2016).
55. Holben, B. N. *et al.* AERONET—A Federated Instrument Network and Data Archive for Aerosol Characterization. *Remote Sens Environ* **66**, 1–16 (1998).

56. Sinyuk, A. *et al.* The AERONET Version 3 aerosol retrieval algorithm, associated uncertainties and comparisons to Version 2. *Atmos Meas Tech* **13**, 3375–3411 (2020).
57. Dubovik, O., Holben, B., Eck, T. F., Smirnov, A. & et Al., Y. K. Variability of absorption and optical properties of key aerosol types observed in worldwide locations. *Journal of Atmospheric Science* 590–608 (2002).
58. Schuster, G. L., Dubovik, O. & Arola, A. Remote sensing of soot carbon - Part 1: Distinguishing different absorbing aerosol species. *Atmos Chem Phys* **16**, 1565–1585 (2016).
59. Kok, J. F. *et al.* Desert dust exerts a substantial longwave radiative forcing missing from climate models. *EarthArXiv* 1–62 (2025)
doi:<https://doi.org/10.31223/X53B2J>.